Available online at www.sciencedirect.com
ScienceDirect
Journal of the European Ceramic Society 31 (2011) 2965–2973
www.elsevier.com/locate/jeurceramsoc

Synthesis and multiferroism in mechanically processed $BiFeO_3$–$PbTiO_3$ ceramics

Valdirlei Fernandes Freitas [a], Luiz Fernando Cótica [a], Ivair A. Santos [a,*], Ducinei Garcia [b], José Antônio Eiras [b]

[a] Grupo de Desenvolvimento de Dispositivos Multifuncionais, Departamento de Física, Universidade Estadual de Maringá, 87020-900 Maringá, PR, Brazil
[b] Grupo de Cerâmicas Ferroelétricas, Departamento de Física, Universidade Federal de São Carlos, 13565–905 São Carlos, SP, Brazil

Received 1 September 2010; received in revised form 1 July 2011; accepted 10 July 2011
Available online 2 August 2011

Abstract

In this study, $(1-x)BiFeO_3$–$(x)PbTiO_3$ multiferroic ceramics, with $x = 0, 0.1, 0.2, 0.25, 0.3$ and 0.4, were processed through high-energy ball milling followed by reactive sintering in air atmosphere. The optimization of the procedure for the preparation of highly-dense $(1-x)BiFeO_3$–$(x)PbTiO_3$ ceramics was carefully investigated and structural/microstructural effects on ferroic properties were carefully addressed. Shrinkage dilatometric measurements revealed an expansion related to a sintering reaction that has occurred before densification. This sintering behaviour was highly $PbTiO_3$ concentration-dependent. The sintering mechanism was found to be directly related with the aliovalent substitution of Pb and Ti ions on A and B sites of the perovskite structure. The obtained ceramics were confirmed as ferroelectric ordered in ferroelectric characterizations. Remnant polarizations and coercive fields greatly dependent on grain size distribution and aliovalent substitutions were revealed. The magnetic hysteresis displayed a weak-ferromagnetic behaviour in all studied samples.

Keywords: C. Ferroelectric properties; C. Magnetic properties; High-energy ball milling

1. Introduction

Multifunctional materials are classified as compounds that have more than one technological applicability and/or property. These appear as potential candidates for revolutionary technological applications in smart devices, as shape memory, electrostrictive, and magnetorheological devices.[1,2] In particular, the multiferroic magnetoelectric materials, whose polarization and magnetization can be simultaneously found, have attracted much academic and technological attention.[3,4] In fact, they can be used in advanced electronic devices, as multiple state memories[5,6] and high-power solid state transformers, fundamentally exploiting the magnetoelectric coupling.[7] Considering magnetoelectric materials, $BiFeO_3$ (BF) is a well-known multiferroic magnetoelectric presenting two ferroic orders, i.e., antiferromagnetic and ferroelectric; in the same phase.[8,9] BF possesses a rhombohedral distorted perovskite structure (R3c space group), a ferroelectric Curie temperature at $T_C \sim 830\,^{\circ}C$, an antiferromagnetic Néel temperature at $T_N \sim 367\,^{\circ}C$,[10,11] excellent ferroelectric properties and magnetoeletric coupling (dE/dH as high as 3 V/cm Oe).[12]Despite having exceptional dielectric and ferroelectric properties, single-phased BF ceramics does not have good electrical resistivity. In fact, elevated conductivity in ceramics confuses the measurement of their electrical properties. Thus, a solution that diminishes the conductivity besides an improvement of electrical and magnetic properties of BF is remarkably desirable. This improvement can be reached with an arrangement of BF in solid solutions, notably with materials previously known for their excellent properties (ferroelectric or magnetic) and high electrical resistivity. In this sense, lead titanate, $PbTiO_3$ (PT), which is a well-known piezoelectric compound - has a tetragonal distorted perovskite structure (P4mm space group) and a ferroelectric phase transition at $T_C \sim 490\,^{\circ}C$[13,14] - seems to present the necessary qualifications to fill these fundamental lacks.[15,16] However, in spite of PT properties, the most commercially exploited and

* Corresponding author. Tel.: +55 44 30115914; fax: +55 44 32634623.
E-mail addresses: freitas@dfi.uem.br (V.F. Freitas), lfcotica@pq.cnpq.br (L.F. Cótica), iasantos@dfi.uem.br (I.A. Santos), ducinei@df.ufscar.br (D. Garcia), eiras@df.ufscar.br (J.A. Eiras).

0955-2219/$ – see front matter © 2011 Elsevier Ltd. All rights reserved.
doi:10.1016/j.jeurceramsoc.2011.07.013

employed piezoelectric material is the lead zirconate titanate (PZT). The main technologically applied PZT compositions are near a not completely understood morphotropic phase boundary (MPB) between the rhombohedral and the tetragonal phases. These compositions possess some of the highest piezoelectric coefficients found in the literature.[17] Following the same idea that for PZT and also an attempt to reduce resistivity and improve the ferroelectric properties of BF, some researchers had been developing the $(1-x)BiFeO_3$–$(x)PbTiO_3$ solid solutions [$(1-x)$BF–(x)PT].[18] These obtained compounds' present ferroelectric, magnetic and piezoelectric characteristics, and also a MPB near 70 wt.% of BF.[18]

This way, the BF–PT solid solutions can be considered an alternative among piezoelectric and ferroelectric materials that can be used in advanced technological applications.[17,19] To date, the BF–PT ceramics are promising candidates to be applied in high temperature piezoelectric devices, with potential applicability in electromechanical transducers and high-power solid state transformers.[20,21] However, the routes employed for processing BF–PT ceramics, and also the correlated characterizations, deserve special attention from the scientific community because those materials acquire properties of both end members, BF and PT. BF–PT system became compounds with high ferroelectric temperature transition ($T_C \sim 632\,^\circ$C) in the MPB region,[15,16] and also remain weak-ferromagnetic at high temperatures ($T_N \sim 377\,^\circ$C).[28] These properties provide potential advanced piezoelectric applications to BF solid solutions, once the vibration frequencies of piezodevices could be hypothetically tuned by applying external magnetic fields, i.e., employing the intrinsic magnetoelectric coupling.[22] Nevertheless, high-performance BF–PT piezoceramics are very difficult to process by using the conventional ceramic method,[23] because these ceramics request special characteristics, as high density, low porosity, high dielectric breakdown, and high electrical resistance; which are necessary conditions for poling those piezoceramics.[24] In addition, a rigorous control of the tetragonality factor (ratio between the c and a parameters in the tetragonal unit cell) should be done in BF–PT piezoceramics, whereas the large lattice anisotropy, caused by PT substitution ($c/a = 1.064$ for PT), can lead the ceramic bodies to be brittle.[25,26]

In this sense, some works have been conducted addressing structural and microstructural issues concerning the production of BF–PT ceramics.[27] In this context, high total apparent densities (although lower than 95%) have been reached for BF–PT ceramics processed by the conventional ceramic method, where high resistivity, at around $10^9\ \Omega$m, were obtained.[28] The tetragonality factor of the $(1-x)$BF–(x)PT solid solutions was also the focus of investigations through X-ray diffraction, revealing tetragonalities as high as 18% for $x = 0.3$.[29] Lately, the morphotropic phase boundary (MPB) of BF–PT ceramics obtained by the solid-state reaction route was carefully determined through X-ray diffraction.[30] In fact, for $x < 0.2$, the $(1-x)$BF–(x)PT solid solutions assume a rhombohedral symmetry (R3m), while for $x > 0.4$ the system adopts a tetragonal symmetry (P4mm). The MPB region, where the two symmetries (rhombohedral and tetragonal) coexist, was found for $0.2 < x < 0.4$.[30]

Evaluating nonconventional routes for processing multiferroic compounds, the high-energy ball milling technique was recently used by Comyn et al.[31] to process adequately high-resistive BF–PT ceramics ($\sim$140 MΩm at 100 °C and 4 MΩm at 150 °C). The microstructure of $(1-x)$BF–(x)PT pellets (the powders were obtained by attrition milled mixed oxides) was investigated by Woodward et al.[18] through scanning electron microscopy (SEM), revealing grains ($\sim$1 μm) with no preferred growth direction, and small porosity. Correas et al.[32] applied mechanosynthesis and spark-plasma sintering for processes dense, homogeneous and nanosized BF–PT ceramics at relatively low temperatures. The effect of Sm doping on the densification behaviour of BF–PT ceramics processed by high-energy ball milling were also investigated by Chu et al.,[26] resulting in ceramics with elevated total apparent density (7.5 g/cm^3 for samples sintered at 1100 °C) and narrow grain size distribution ($\sim$1 μm). In fact, Cheng et al.[33] promoted SEM analyses on (0.7)$BiGa_{0.05}Fe_{0.95}$–(0.3)PT fractured surfaces that showed noticeable more transgranular fractures than intergranular ones, indicating that small isovalent modification on B site of the perovskite structure can contribute to enhance the densification rates.[33] Electrical characterizations, as a function of electric field and temperature, were conducted in (0.7)BF–(0.3)PT ceramics, exhibiting their ferroelectric nature with remnant polarization of 6 μC/cm^2 and $T_C \sim 650\,^\circ$C.[28,33] Recently, Freitas et al.[34] reported piezoelectric coefficients as high as those found for PZT ceramics in high-energy ball milled (0.6)BF–(0.4)PT samples.

Taking the scientific and technological requests for processing high-quality BF–PT ceramics, some issues concerning the protocols used to synthesize highly dense BF–PT ceramics still need to be investigated to optimize these processes. Even though, promising BF–PT piezoceramics demand a slight control of their microstructural and structural characteristics. Moreover, a rigorous control of their electrical conductivities, obtained mainly through microstructural controlling, needs to be achieved for poling BF–PT ceramics. With these questions in mind, in this work, thermal, structural, microstructural, ferroelectric and magnetic investigations in $(1-x)$BF–(x)PT ceramics, synthesized by high-energy ball milling, were carried out. The samples were carefully investigated through X-ray diffraction, scanning electron microscopy, dilatometric measurements, differential scanning calorimetry, ferroelectric hysteresis measurements and magnetic hysteresis measurements. Dense BF–PT ceramics (>90% of the theoretical density), with narrow grain size distribution (with average grain sizes decreasing with x from $\sim$8 until 1 μm) of morphologically homogeneous grains, and electrical resistivity higher then $10^6\ \Omega$m, were obtained for samples where the sintering time and temperature showed to be highly dependent on the PT content in the BF–PT solid solution. Ferroelectric hysteresis loops revealed ferroelectrically ordered samples, with remnant polarizations and coercive electric fields as high as 2.5 μC/cm^2 and 22.5 kV/cm, respectively. The magnetic hysteretic loops revealed typical weak ferromagnetic magnetic behaviour in all studied samples.

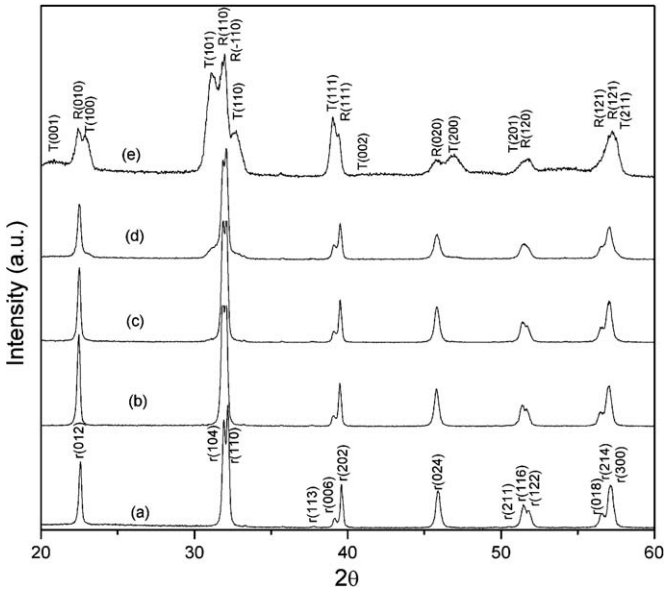

Fig. 1. X-ray diffraction patterns for high-energy ball milled (1 h) BF–PT powders annealed at 950 °C for 1 h. r = R3c, R = R3m and T = P4mm space groups. (a) (0.9)BF–(0.1)PT; (b) (0.8)BF–(0.2)PT; (c) (0.75)BF–(0.25)PT; (d) (0.7)BF–(0.3)PT, and (e) (0.6)BF–(0.4)PT.

2. Experimental

Stoichiometric powders of $(1-x)BiFeO_3$–$(x)PbTiO_3$ compounds, with nominal compositions of $x = 0$, 0.1, 0.2, 0.25, 0.3 and 0.4, were synthesized from analytical graded (Aldrich) Bi_2O_3, Fe_2O_3, La_2O_3, PbO and TiO_2 precursors. These powders were mechanically processed by high-energy ball milling (HEBM), with a Retsch PM100 planetary ball mill, using vial (80 cm^3 of volume) and balls (10 mm of diameter) of hardened steel, in air atmosphere, as previously reported.[35,36] The optimized milling conditions were: ball-to-powder mass ratio (30:1), milling speed (32 rad s^{-}) and time (1 h). After milling, the powders were separated in two parts. The first was annealed at 950 °C for 1 h, while the second one was conformed in disc shapes

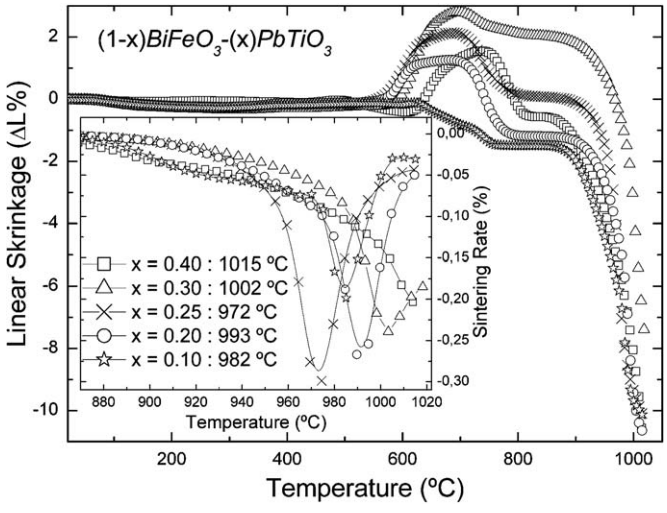

Fig. 2. Linear shrinkage and sintering rate (inset) for high-energy ball milled (1 h) BF–PT samples. Heating rate of 3 °C/min.

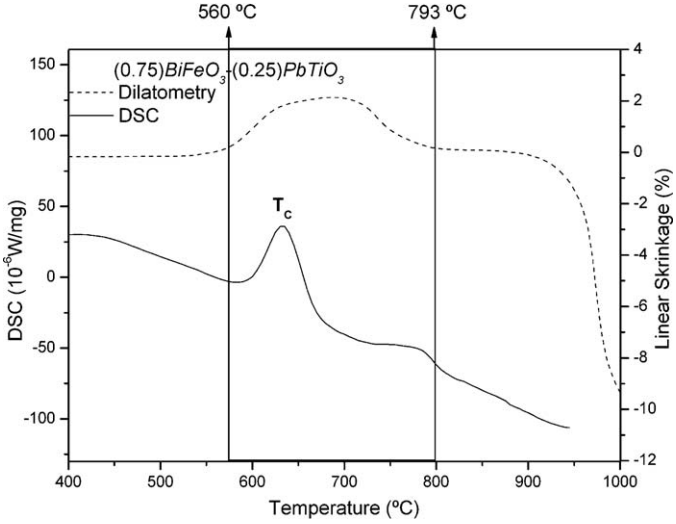

Fig. 3. Differential scanning calorimetry and dilatometric results for the (0.75)BF–(0.25)PT sample. Heating rate of 3 °C/min.

with 6 mm in diameter and 1 mm in thickness. The discs were submitted to cold isostatic pressing (146 MPa) and reactively sintered at different temperatures (from 933 °C to 1075 °C) for different times (from 1 h to 3 h). Only in $x = 0.3$ and 0.4 samples, tiny amounts of La_2O_3 (3 wt.% and 5 wt.%, respectively) were added before sintering to reduces the tetragonality of these samples and to permit subsequent ferroelectric characterization. X-ray diffraction (XRD) analyzes were conducted with a Shimadzu XRD-7000 X-ray diffractometer (Cu k_α radiation). Scanning electron microscopy (SEM) was performed with a Shimadzu SS550 SuperScan scanning electron microscope, equipped with an Energy dispersive X-ray spectroscopy (EDS) detector. Differential scanning calorimetric studies were performed by using a Netzsch STA 409 Luxx equipment, in

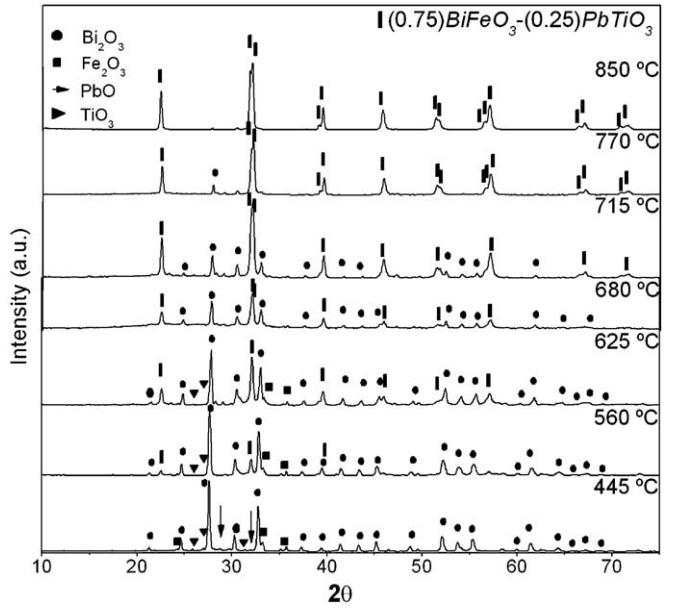

Fig. 4. X-ray diffraction patterns for (0.75)BF–(0.25)PT powders annealed at different temperatures for 1 h.

Table 1
Total apparent density (ρ_A), theoretical density (ρ_{TH}), relative density (ρ_R), rhombohedral (a_{Rh}) lattice parameter, tetragonal a_T and c_T lattice parameters, tetragonality factor ($t = c_T/a_T$), and electrical resistivity (ρ) for BF–PT ceramics sintered at optimized temperatures and times: 0.10: (0.9)BF–(0.1)PT, 982 °C/1 h; 0.20: (0.8)BF–(0.2)PT, 1043 °C/2 h; 0.25: (0.75)BF–(0.25)PT, 1022 °C/2 h; 0.30: (0.7)BF–(0.3)PT, 1052 °C/2 h; and 0.40: (0.6)BF–(0.4)PT, 1065 °C/1 h.

x	ρ_A (g/cm^3)	ρ_{TH} (g/cm^3)	ρ_R	a_{Rh} (Å)	a_T (Å)	c_T (Å)	t	ρ (M Ωm)
0.10	7.55 ± 0.03	8.42 ± 0.01	0.90 ± 0.07	3.948(1)	3.982(8)	4.042(8)	1.015	1.84
0.20	7.60 ± 0.03	8.23 ± 0.01	0.92 ± 0.08	3.972(9)	3.862(8)	4.271(1)	1.105	6.22
0.25	7.50 ± 0.03	8.32 ± 0.02	0.90 ± 0.09	3.951(1)	3.812(2)	4.566(5)	1.197	4.37
0.30	7.55 ± 0.02	8.45 ± 0.04	0.89 ± 0.08	3.934(8)	3.802(1)	4.503(5)	1.184	5.21
0.40	7.75 ± 0.02	8.36 ± 0.04	0.93 ± 0.07	3.944(7)	–	–	–	4.36

air flux and a heating/cooling rate of 10 °C/min. Dilatometric measurements were performed with a Netzsch dilatometer (Dil 402-PC) in air flux and at a heating rate of 3 °C/min. The electrical resistivity of ceramics was determined using a LCR bridge (Agilent E4980). Grain size distributions were determined analyzing SEM images and applying the standard circular method.[37] Total apparent densities (ρ_{AP}) were determined by applying the Arquimedes method in distilled water, while the theoretical densities (ρ_{TH}) were calculated from the lattice parameters obtained from the X-ray diffraction patterns and the respective molecular weight of the batch formula. The relative total apparent densities ($\rho_R = \rho_{AP}/\rho_{TH}$) were calculated using the total apparent and theoretical densities. The ferroelectric hysteresis loops were collected with a Sawyer-Tower circuit at 60 Hz. The magnetic hysteresis loops were obtained by using a LakeShore (7307-7 Inch) vibrating sample magnetometer.

3. Results and discussion

3.1. Structural and calorimetric characterisations

Fig. 1 shows the XRD profiles for $(1-x)$BF–(x)PT powders submitted to high-energy ball milling, and heat treated at 950 °C for 1 h. In contrast with Zhu et al.,[30] which report a MPB since $x = 0.2$, here samples with $x = 0.1$, 0.2, and 0.25 only had crystallized in the rhombohedral perovskite structure (R3c space group). However, for $x = 0.3$, and 0.4 samples, rhombohedral (R3m) and tetragonal (P4mm) phases could be identified, corroborating with the existence of a morphotropic phase boundary (MPB) in this system.[20,30] It is worth noting that formation of BF–PT compounds take place at temperatures very lower than those used in conventional ceramic method.[30] These results are a clear indicative that the employed milling time makes these samples reach the first mechanical alloying stage.[35,36] In this stage, the starting oxides were highly lowered in both particle and crystallite sizes, so that the final crystallization process could be reached by using heat treatments at lower temperatures for short times, as indicated in Fig. 1.

The dilatometric results (linear shrinkage and sintering rate) for as-milled and subsequently cold pressed BF–PT samples are presented in Fig. 2. In this work, the starting points for sintering studies were the maximum contractions obtained in dilatometric studies (inset). As can be seen, an almost linear correlation between the temperatures of maximum contraction and the PT concentration was observed. In fact, for each specific PT concentration there is just one appropriate sintering temperature. These results contrast with those reported in the literature, where none differences in the temperatures of sintering, referring to the PT concentrations, was observed or pointed out for conventionally processed samples.[28,33] In this way, studies concerning optimization of sintering temperatures of BF–PT ceramics need to be conducted carefully, whereas the presence of more than one factor, as crystal symmetries with possible habit for grain growth (P4mm, for example), can affects the sintering kinetics. Also, dilatometric results indicate the possible existence of different activation energies for active sintering processes in BF–PT solid solutions, which can be directly related with the dissimilar ionic ratios and valence numbers of the Bi and Pb (perovskite A site) and Fe and Ti (perovskite B site) ions. In fact, the gain of energy provided by the mechanical activation (high-energy ball milling) is almost the same for all studied samples, i.e., they reached the first mechanical alloying stage. These differences in activation energies can affect the grain growth mechanism for each sample, leading to different grain sizes distribution, as revealed by the SEM and XRD analyses discussed below.

The differential scanning calorimetry signal and the linear shrinkage, for the (0.75)BF–(0.25)PT sample, is shown in

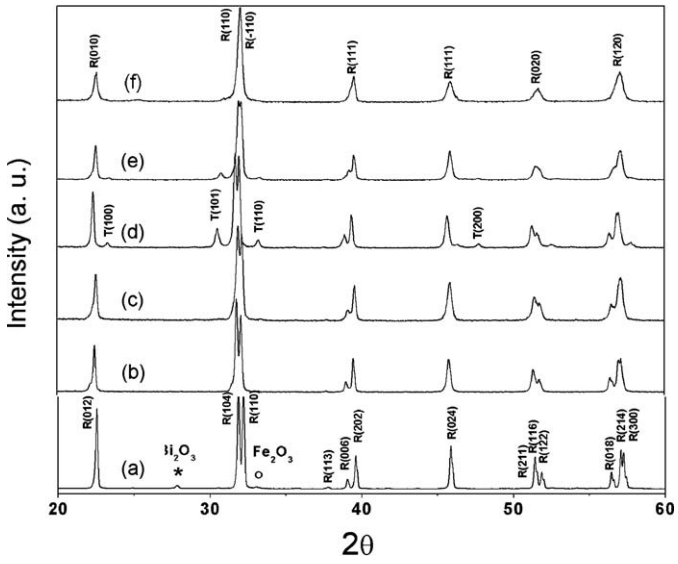

Fig. 5. XRD patterns for BF–PT ceramics sintered at optimized temperatures and times: (a) $BiFeO_3$–900 °C/1 h; (b) (0.9)BF–(0.1)PT, 982 °C/1 h; (c) (0.8)BF–(0.2)PT, 1043 °C/2 h; (d) (0.75)BF–(0.25)PT, 1022 °C/2 h; (e) (0.7)BF–(0.3)PT, 1052 °C/2 h; and (f) (0.6)BF–(0.4)PT, 1065 °C/1 h.

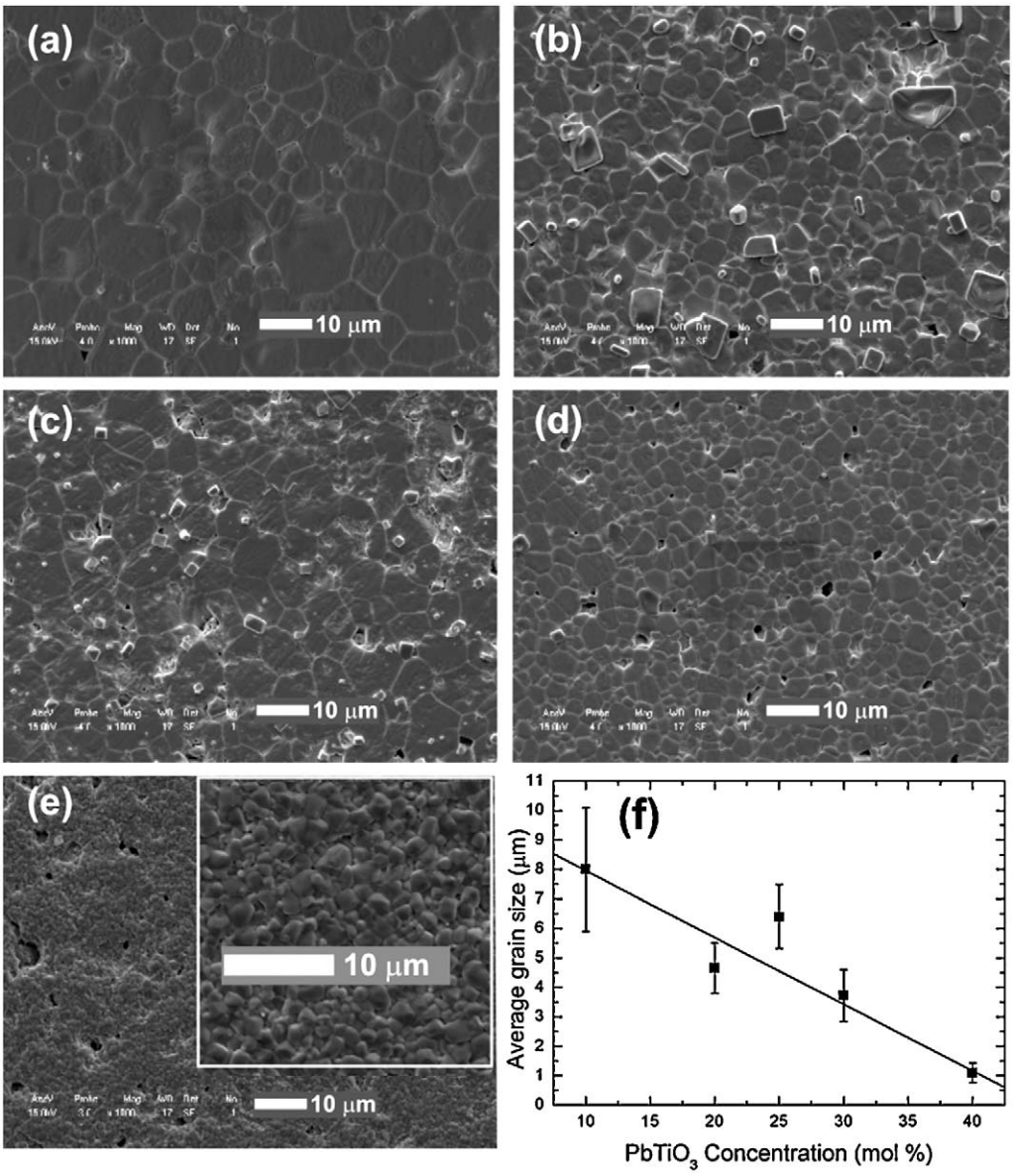

Fig. 6. Scanning electron microscope images for thermal attacked surfaces of BF–PT ceramics sintered at optimized temperatures and times: (a) (0.9)BF–(0.1)PT, 982 °C/1 h; (b) (0.8)BF–(0.2)PT. 1043 °C/2 h; (c) (0.75)BF–(0.25)PT, 1022 °C/2 h; (d) (0.7)BF–(0.3)PT, 1052 °C/2 h; and (f) mean grain size as a function of the PT concentration.

Fig. 3. The curves shown, which are representative for all studied samples, reveal anomalous dilatation occurring at temperatures between 550 °C and 800 °C, which are also shown in Fig. 2. It is worth noting that in this same temperature range, two endothermic peaks also appear in the DSC curve (Fig. 3). Taking this observation into account, the thermal kinetics for phase formation in the 0.75BF–0.25PT sample was investigated through XRD analysis. The XRD results, obtained for sample batches heat-treated at different temperatures for 0.5 h, are shown in Fig. 4. As can be observed, the rhombohedral 0.75BF–0.25PT phase starts at temperatures as low as 580 °C, and is completely formed at 850 °C. Then, BF–PT compounds were stabilized directly from oxide precursors, avoiding undesirable phases. These results also corroborate with our previous XRD analysis, where no spurious or residual phases were observed in powders heat treated at 950 °C for 1 h (see Fig. 1). In this way, the thermal expansion observed in dilatometric curves (Figs. 2 and 3) can be associated with the sintering reaction towards BF–PT compounds directly from oxide precursors in partially reacted mixture. As BF–PT compounds have molar volume higher than those of oxide precursors, a thermal expansion would be expected, corroborating with previous reports concerning the synthesis of lead titanate zirconate (PLZT) and lead zirconium niobate–titanate (PZN–PT) by high-energy ball milling.[38,39]

The X-ray diffraction patterns for BF–PT ceramics, sintered at optimized temperature and time, are shown in Fig. 5. In this figure, most of phases were indexed as being rhombohedral (R3m or R3c) perovskite. The tetragonal profiles (P4mm) were identified in all patterns, except for $x = 0.4$. In $x = 0.3$ and 0.4 sam-

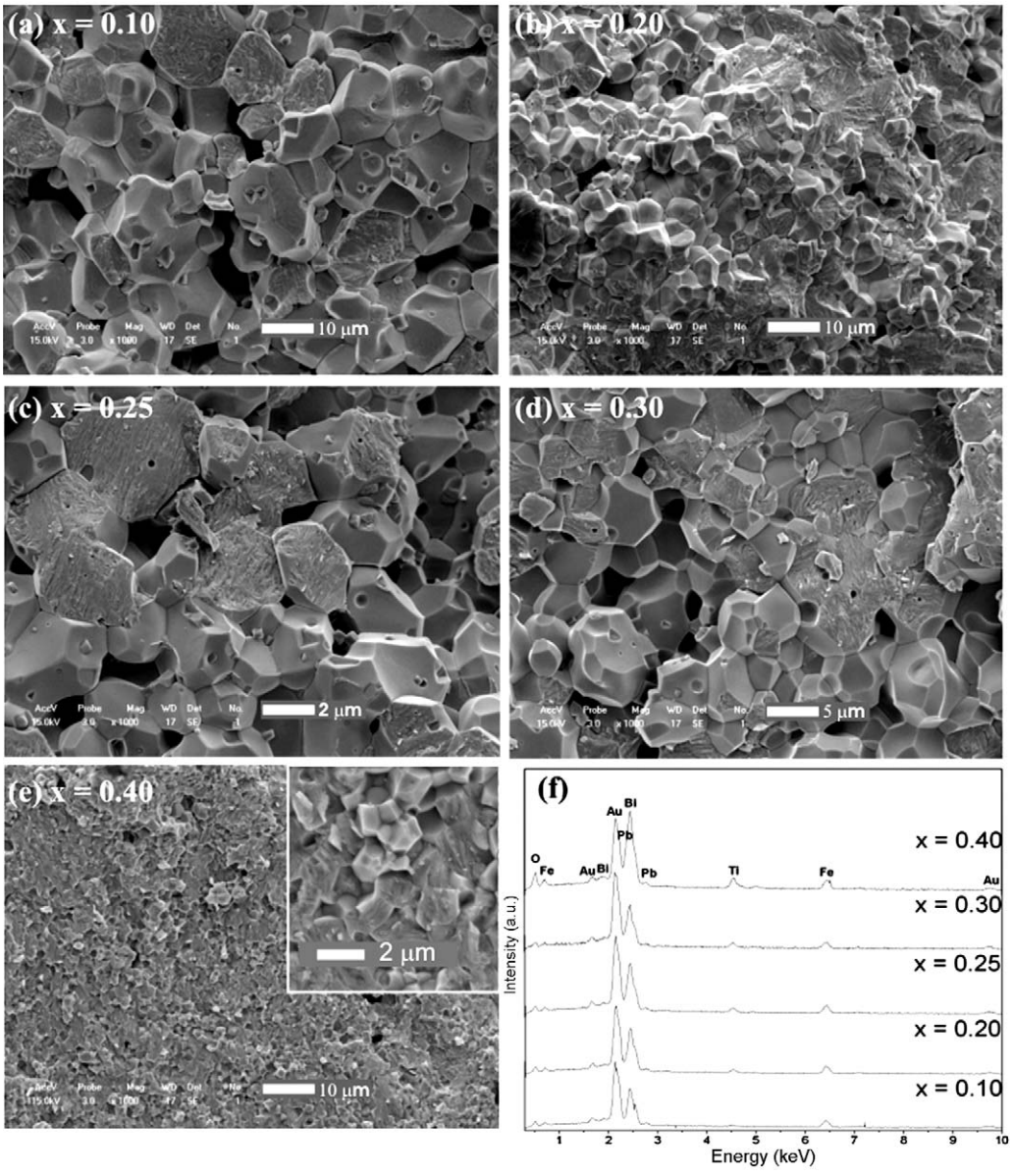

Fig. 7. Scanning electron microscope images for fractured BF–PT ceramics sintered at optimized temperatures and times: (a) (0.9)BF–(0.1)PT, 982 °C/1 h; (b) (0.8)BF–(0.2)PT, 1043 °C/2 h; (c) (0.75)BF–(0.25)PT, 1022 °C/2 h; (d) (0.7)BF–(0.3)PT, 1052 °C/2 h; and (f) energy dispersive X-ray results for BF–PT ceramics.

ples tiny amounts of La_2O_3 (3 wt.% and 5 wt.%, respectively) were added to guarantee ferroelectric characterizations. In fact, when $x = 0.3$ and 0.4 compositions without La are sintered at optimized temperatures (as those obtained from the previous dilatometric investigations) the tetragonal phase emerges with a very high tetragonality that causes microstructural instability, which become these samples highly brittle, preventing the subsequent ferroelectric characterization. In this way, the La addition is necessary considering the ferroelectric characterization. The rhombohedral and tetragonal lattice parameters, as well as the tetragonality factors, are listed in Table 1. It is worth noting that the tetragonal a lattice parameter (a_T) decreases with the increase of the PT concentration, while the tetragonal c ones (c_T) increase. It is important to mention that those samples with $x = 0.25$ and 0.3 reached tetragonalities as high as ~18% (Table 1). However, these samples were not brittle, as reported by Cheng et al.[40] In face of results, the synthesis mechanism for phase formation in BF–PT system can be considered as being fundamentally controlled by the aliovalent substitutions on A and B sites of the perovskite structure once these samples were submitted to the same milling protocol. In this way, the densification behaviour favours to be affected by the coexistence of tetragonal and rhombohedral phases, as evidenced by as follows presented SEM investigations.

3.2. Densification behaviour

The SEM images, for polished and thermal attacked ceramic surfaces, are shown in Fig. 6(a)–(e). Morphologically homoge-

neous grains and narrow grain size distribution can be observed in each case. The PT content dependence on average grain sizes, obtained from the analysis of the surface in the SEM images by using the circular method,[37] is shown in Fig. 6(f). As the average grain size tends to decrease almost linearly with PT content (Fig. 6(e)), this result indicates that the aliovalent substitution of Bi for Pb, and Fe for Ti, in A and B perovskite sites, respectively, contribute to prevent the grain growth fundamentally through the formation of tetragonal phase. These results are in accordance with those obtained in the XRD analyses and indicate that the average grain sizes turn to decrease with the increase of the tetragonality factor and aliovalent substitution in BF–PT ceramics.

The densification studies, which resulted in the theoretical and apparent densities listed in Table 1, revealed high-dense BF–PT ceramics, with relative densities reaching 93% of theoretical ones. The lower total apparent density obtained in this work ($\rho_A > 7.55$ g/cm^3), was still higher than those obtained by Zhang et al. ($\rho_A > 7.5$ g/cm^3).[15] Interesting, the densification data contrast with those obtained by SEM, whereas the ceramic which presented an elevated quantity of surface porous ($x = 0.4$) was those that presented the higher relative density. This result is related with internal porous in ceramics, as evidenced by the surface fracture analysis shown in Fig. 7. As can be observed, for lower PT concentrations the intergranular fractures are majority (Fig. 7(a) and (b)), indicating the existence of possible amorphous or spurious phases at the grains boundary. In fact, for high PT concentrations the transgranular fractures are predominant (Fig. 7(d) and (e)). The chemical analysis (EDS) performed in fractured surfaces (Fig. 7(f)) reveal stoichiometries very close to nominal values.

3.3. Ferroelectric and magnetic properties

The Fig. 8 shows the polarization loops measured at different temperatures for sintered BF–PT ceramics, as examples of their ferroelectric behaviour. This figure reveals clear hysteretic ferroelectric loops with remnant polarizations and coercive fields ranging from 0.1 μC/cm^2 to 17 μC/cm^2 and from 4.5 kV/cm to 20 kV/cm, respectively, and that the coercive field and remnant polarization had increased with the increase of the PT content. Recently, Sakamoto et al.[41] demonstrated, through low and room temperature polarization loop measurements that ferroelectric characterization conducted at low temperatures prevent the detrimental electrical conductivity effects observed in BF–PT thin films. As the ferroelectric characterisation results presented in Fig. 8 were also obtained at relatively high electric fields (as high as 60 kV/cm), we believe that, in spite of the relative low electrical resistivity of high-energy ball milled BF–PT samples, the ferroelectric loops shown in this figure are in fact ferroelectric, with minor contributions of capacity losses. Also, similar results were also obtained at 10 Hz for (0.7)Bi[$Ga_{0.1}Fe_{0.9}$]O_3–(0.3)$PbTiO_3$ ($P_r \sim 0.5$ μC/cm^2) and (0.6)Bi[$Ga_{0.4}Fe_{0.6}$]O_3–(0.4)$PbTiO_3$ ($P_r \sim 0.4$ μC/cm^2) compounds processed by the conventional ceramic route,[29] attesting the ferroelectric characteristics of the BF–PT samples obtained by high-energy ball milling. However, no direct correlation between electrical resistivities (Table 1) and coercive field or remnant polarization was observed.

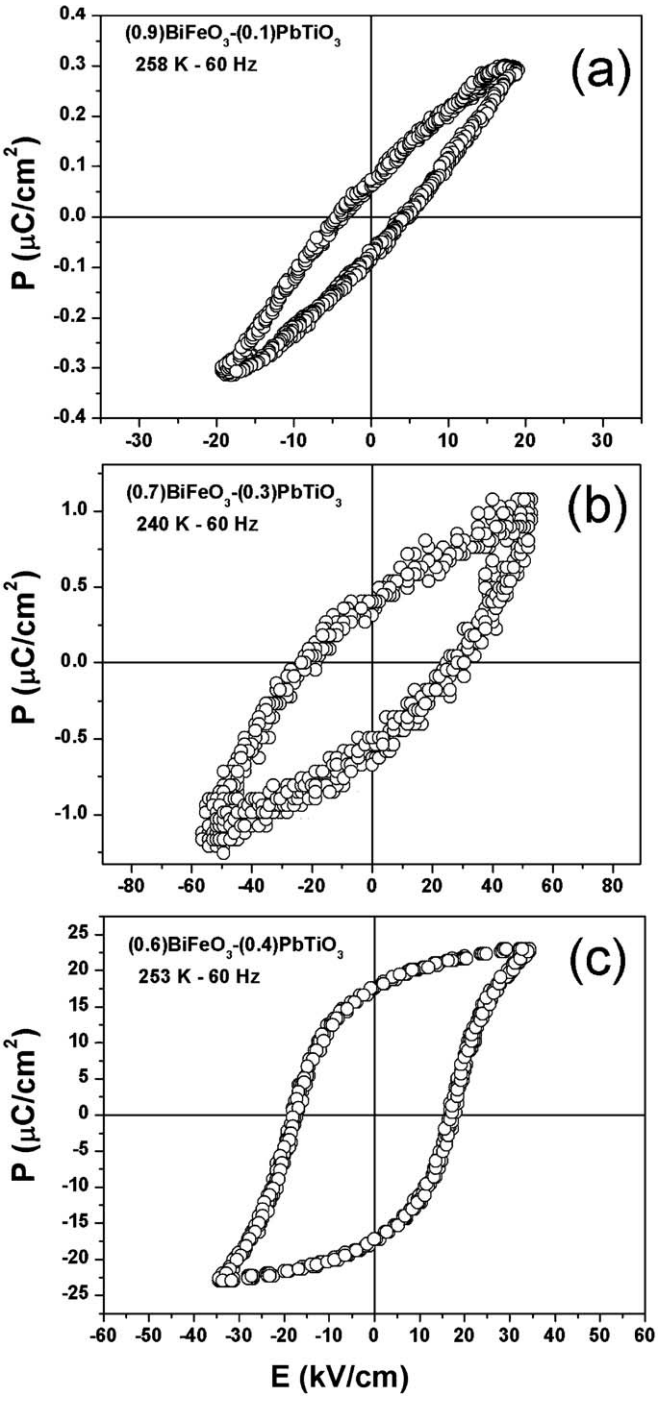

Fig. 8. Ferroelectric hysteretic loops (60 Hz) at different temperatures for BF–PT ceramics sintered at optimized temperatures and times: (a) (0.9)BF–(0.1)PT, 982 °C/1 h; (b) (0.7)BF–(0.3)PT, 1052 °C/2 h; and (c) (0.6)BF–(0.4)PT, 1065 °C/1 h.

Fig. 9 shows magnetic hysteretic loops for $(1-x)BiFeO_3$–$(x)PbTiO_3$ ($x = 0.1$, 0.2, 0.25, 0.3, and 0.4) samples. The remnant magnetization as a function of the PT concentration is shown in Fig. 9(a). As can be seen, the remnant magnetization decreases with the increase of the PT concentration. The samples magnetizations were not saturated

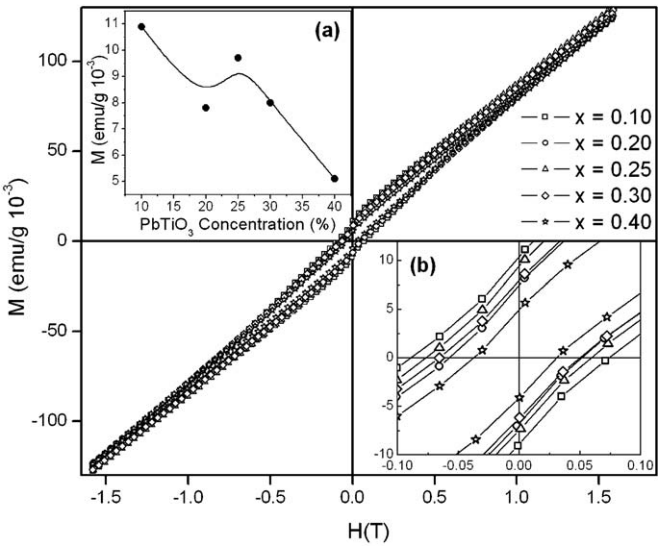

Fig. 9. Magnetic hysteretic loops for BF-PT ceramics sintered at optimized temperatures and times: 0.10: (0.9)BF–(0.1)PT, 982 °C/1 h; 0.20: (0.8)BF–(0.2)PT, 1043 °C/2 h; 0.25: (0.75)BF–(0.25)PT, 1022 °C/2 h; 0.30: (0.7)BF–(0.3)PT, 1052 °C/2 h; and 0.40: (0.6)BF–(0.4)PT, 1065 °C/1 h. Insets: (a) remnant magnetization as a function of the $PbTiO_3$ concentration. (b) Magnetic hysteresis loops evidencing the coercive fields.

with the increase of the magnetic field in the investigated field range, indicating an antiferromagnetic behaviour. However, in all studied samples were observed magnetic hysteresis with remnant magnetizations ranging from 5×10^{-3} emu/g to 10×10^{-3} emu/g (Fig. 9(b)). This magnetic behaviour is commonly described as a weak ferromagnetic order.[40] According to Zhu et al.,[20] the arising of this small magnetic hysteretic behaviour is due to the formation of chemically ordered microregions (magnetic nanoclusters) in BF–PT samples. The freezing in these magnetic nanoclusters would induce the residual magnetization, which is recognized as a weak ferromagnetic response.

4. Conclusions

Dense $(1-x)BiFeO_3$–$(x)PbTiO_3$ ceramics were synthesized by using high-energy ball milling followed by reactive sintering. Their structural, microstructural and ferroelectric properties were carefully investigated. The sintering behaviour of milled powders were also investigated and elucidated by using dilatometric and X-ray diffraction measurements. An anomalous expansion, observed in dilatometric measurements, indicates that the sintering reaction has occurred before densification, which is highly dependent on the PT concentration and aliovalent substitution of Pb and Ti ions on the A and B sites of the perovskite structure. The results also point to structurally relaxed ceramics, with morphologically homogeneous grains of narrow grain size distribution. It was observed that the grain growth mechanism is highly dependent on the structural and chemical nuances, as the existence of a morphotropic phase boundary, tetragonal symmetric phases and aliovalent substitution in (x)BF–(1–x)PT solid solutions. Ferroelectric and magnetic characterizations reveal ferroelectric and weak-ferromagnetic ordered ceramics, with remnant polarization and magnetization, and coercive fields highly dependent on the $PbTiO_3$ concentration. The whole set of results indicate that the obtained samples can be employed as piezodevices once they present ferroelectric and magnetic ordering at room temperature.

Acknowledgements

The authors would like to thank CNPq (proc. 476964/2009-1 and 552900/2009-5), Fundação Araucária de Apoio ao Desenvolvimento Científico e Tecnológico do Paraná (Prots. 10779 and 15727), CAPES (Procad 082/2007), and FAPESP (proc. 2008/04025-0) Brazilian agencies for financial support, and COMCAP/UEM for providing SEM and DSC facilities. V.F.F. also thanks CNPq for fellowship.

References

1. Kumar A, Podraza NJ, Deneb S, Li J, Martin LW, Chu Y-H, Ramesh R, Collins RW, Gopalan V. Linear and nonlinear optical properties of $BiFeO_3$. *Appl Phys Lett* 2008;**92**:231915.
2. Lin Y, Sodano HA. Concept and model of a piezoelectric structural fiber for multifunctional composites. *Compos Sci Technol* 2008;**68**:1911–8.
3. Ramesh R, Spaldin NA. Multiferroics: progress and prospects in thin films. *Nat Mater* 2007;**6**:21–9.
4. Béa H, Paruch P. Multiferroics: a way forward along domain walls. *Nat Mater* 2009;**8**:168–9.
5. Bibes M, Barthelemy A. Multiferroics: towards a magnetoelectric memory. *Nat Mater* 2008;**7**:425–6.
6. Scott JF. Data storage: multiferroic memories. *Nat Mater* 2007;**6**:256–7.
7. Neaton JB, Ederer C, Waghmare UV, Spaldin NA, Rabe KM. First-principles study of spontaneous polarization in multiferroic $BiFeO_3$. *Phys Rev B* 2005;**71**:014113.
8. Ederer C, Spaldin NA. Weak ferromagnetism and magnetoelectric coupling in bismuth ferrite. *Phys Rev B* 2005;**71**:060401.
9. Higuchi T, Liu H-S, Yao P, Glans P-A, Guo J, Chang C, Wu Z, Sakamoto W, Itoh N, Shimura T, Yogo T, Hattori T. Electronic structure of multiferroic $BiFeO_3$ by resonant soft X-ray emission spectroscopy. *Phys Rev B* 2008;**78**:085106.
10. Kamba S, Nuzhnyy D, Savinov M, Sebek J, Petzelt J, Prokleska J, Haumont R, Kreisel J. Infrared and terahertz studies of polar phonons and magnetodielectric effect in multiferroic $BiFeO_3$ ceramics. *Phys Rev B* 2007;**75**:024403.
11. Baetting P, Ederer C, Spaldin NA. First principles study of the multiferroics $BiFeO_3$, Bi_2FeCrO_6, and $BiCrO_3$: structure, polarization, and magnetic ordering temperature. *Phys Rev B* 2005;**72**:214105.
12. Wang J, Neaton JB, Zheng H, Nagarajan V, Ogale SB, Liu B, Viehland D, Vaithyanathan V, Schlom DG, Waghmare UV, Spaldin NA, Rabe KM, Wuttig M, Ramesh R. Epitaxial $BiFeO_3$ multiferroic thin film heterostructures. *Science* 2002;**299**:1719–22.
13. Lee SW, Shim KB, Auh KH, Knott P. Ferroelectric anomaly in the differential thermal analysis of $PbTiO_3$ glass. *Mater Lett* 1999;**38**:356–9.
14. Burnett TL, Comyn TP, Merson E, Bell AJ, Mingard K, Hegarty T, Cain M. Electron backscatter diffraction as a domain analysis technique in $BiFeO_3$–$PbTiO_3$ single crystals. *IEEE Trans Ultrason Ferrolectr Freq Control* 2008;**55**:957–62.
15. Zhang S, Li H, Li M. Size-dependent piezoelectric coefficient d_{33} of $PbTiO_3$ nanoparticles. *Mater Lett* 2008;**62**:2438–40.
16. Khan MA, Comyn TP, Bell AJ. Ferroelectric $BiFeO_3$–$PbTiO_3$ thin films on Pt/Si substrates. *IEEE Trans Ultrason Ferroelectr Freq Control* 2007;**54**:2583–6.
17. Burnett TL, Comyn TP, Bell AJ. Flux growth of $BiFeO_3$–$PbTiO_3$. *J Cryst Growth* 2005;**258**:156–61.

18. Woodward DI, Reaney IM, Eitel RE, Randall CA. Crystal and domain structure of the $BiFeO_3$–$PbTiO_3$ solid solution. *J Appl Phys* 2003;**94**:3313–8.
19. Cheng J, Xing XR, Liu GR, Li JH, Liu YT. Structure and negative thermal expansion in the $PbTiO_3$–$BiFeO_3$ system. *Appl Phys Lett* 2006;**89**:101914.
20. Zhu WM, Ye Z-G. Effects of chemical modification on the electrical properties of $0.67BiFeO_3$–$0.33PbTiO_3$ ferroelectric ceramics. *Ceram Int* 2004;**30**:1435–42.
21. Dong S, Li J-F, Viehland D. Magnetoelectric coupling, efficiency, and voltage gain effect in piezoelectric–piezomagnetic laminate composites. *J Mater Sci* 2006;**41**:97–106.
22. Gotardo RAM, Santos IA, Cótica LF, Botero ER, Garcia D, Eiras JA. Improved ferroelectric and magnetic properties of monoclinic structured $0.8BiFeO_3$–$0.2BaTiO_3$ magnetoelectric ceramics. *Scripta Mater* 2009;**61**:508–11.
23. Leist T T, Jo W, Comyn T, Bell A, Rodel J. Shift in morphotropic phase boundary in La-doped $BiFeO_3$–$PbTiO_3$ piezoceramics. *J Appl Phys* 2009;**48**:120205.
24. Spínola DU, Santos IA, Bássora LA, Eiras JA, Garcia D. Dielectric properties of rare earth doped $(Sr,Ba)Nb_2O_6$ ceramics. *J Eur Ceram Soc* 1999;**19**:1111–4.
25. Ranjan R, Raju KA. Unconventional mechanism of stabilization of a tetragonal phase in the perovskite ferroelectric $(PbTiO_3)_{(1-x)}(BiFeO_3)_{(x)}$. *Phys Rev B* 2010;**82**:05119.
26. Chu S-Y, Chen C-H. Effects of dopants on the piezoelectric and dielectric properties of Sm-modified $PbTiO_3$ ceramics. *Mater Res Bull* 2000;**35**:2317–24.
27. Bhattacharjee S, Pandey D. Stability of the various crystallographic phases of the multiferroic $(1-x)BiFeO_3$–$xPbTiO_3$ system as a function of composition and temperature. *J Appl Phys* 2010;**107**:124112.
28. Comyn TP, McBride SP, Bell AJ. Processing and electrical properties of $BiFeO_3$–$PbTiO_3$ ceramics. *Mater Lett* 2004;**58**:3844–6.
29. Sunder VS, Halliyal A, Umarji AM. Investigation of tetragonal distortion in the $PbTiO_3$–$BiFeO_3$ system by high-temperature X-ray diffraction. *J Mater Res* 1995;**10**:1301–6.
30. Zhu W-M, Guo H-Y, Ye Z-G. Structural and magnetic characterization of multiferroic $(BiFeO_3)_{1-x}(PbTiO_3)_x$ solid solutions. *Phys Rev B* 2008;**78**:014401.
31. Comyn TP, Stevenson T, Bell AJ. Piezoelectric properties of $BiFeO_3$–$PbTiO_3$ ceramics. *J Phys IV* 2005;**128**:13–7.
32. Correas C, Hungria T, Castro A. Mechanosynthesis of the whole $xBiFeO_3$–$(1-x)PbTiO_3$ multiferroic system: structural characterization and study of phase transitions. *J Mater Chem* 2011;**21**:3125–32.
33. Cheng J-R, Li N, Cross LE. Structural and dielectric properties of Ga-modified $BiFeO_3$–$PbTiO_3$ crystalline solutions. *J Appl Phys* 2003;**94**:5153–9.
34. Freitas VF, Santos IA, Botero E, Fraygola BM, Garcia D, Eiras JA. Piezoelectric characterization of $(0.6)BiFeO_3$–$(0.4)PbTiO_3$ multiferroic ceramics. *J Am Ceram Soc* 2011;**94**:754–8.
35. Freitas VF, Grande HLC, Medeiros SN, Santos IA, Cótica LF, Coelho AA. Structural, microstructural and magnetic investigations in high-energy ball milled $BiFeO_3$ and $Bi_{0.95}Eu_{0.05}FeO_3$ powders. *J Alloys Compd* 2008;**461**:48–52.
36. Santos IA, Grande HLC, Freitas VF, Medeiros SN, Paesano A, Cótica LF, Radovanovic E. Structural, microstructural and Mössbauer spectral study of the $BiFe_{1-x}Mn_xO_3$ mechanosynthesized system. *J Non-Cryst Solids* 2006;**352**:3721–4.
37. Abrans H. Grain size measurement by the intercept method. *Metallography* 1971;**4**:59–78.
38. Lente MH, Guerra JDS, de GKS, Souza BM, Fraygola CFV, Raigoza D, Garcia JA, Eiras. Nature of the magnetoelectric coupling in multiferroic $Pb(Fe_{1/2}Nb_{1/2})O_3$ ceramics. *Phys Rev B* 2008;**78**:054109.
39. Kong LB, Ma J, Zhu W, Tan OK. Preparation and characterization of PLZT(8/65/35) ceramics via reaction sintering from ball milled powders. *Mater Lett* 2002;**52**:378–87.
40. Cheng J, Yu S, Chen J, Meng Z, Cross LE. Dielectric and magnetic enhancements in $BiFeO_3$–$PbTiO_3$ solid solutions with La doping. *Appl Phys Lett* 2006;**89**:122911.
41. Sakamoto W, Iwata A, Yogo T. Ferroelectric properties of chemically synthesized perovskite $BiFeO_3$–$PbTiO_3$ thin films. *J Appl Phys* 2008;**104**:104106.